Optimisation of an Air Lubrication System for Geometry and Topology: A Proposed Solution for Ship Retrofitting

Hannes Renzsch, FRIENDSHIP-SYSTEMS, Potsdam/Germany, renzsch@friendship-systems.com
Andrew Spiteri, LJMU, Liverpool/UK, A.Spiteri@ljmu.ac.uk
Milad Armin, ENKI Marine, Liverpool/UKm.armin@enkimarine.co.uk
Eduardo Blanco-Davis, LJMU, Liverpool/UK, e.e.blancodavis@ljmu.ac.uk
Alex Routledge, Armada Technologies, Birkenhead/UK, alex.routledge@armada-technologies.com

Abstract

This paper presents the challenges of developing and optimising a second-generation Passive Air Lubrication System (PALS). After presenting the general working principle of this system, the paper focuses on the geometry optimisation of the system itself and the arrangement in the vessel. The challenges and limitations of the associated CFD computations will be discussed. Experimental test results under laboratory conditions and validation of the system's design will be presented qualitatively. An exemplary arrangement for a PALS will be shown.

1. The Challenge

Recent and future regulations require significantly reduced emissions from merchant shipping, *IMO (2023*). While current and emerging technologies offer quite a range of options for new-builds, these are considerably more limited for vessels already in operation.

One of these options available to vessels in service is to reduce the required propulsive power –and consequently fuel consumption and emissions– by reduction of resistance, e.g., by using air lubrication. Installation of an air lubrication system in an existing ship poses the dual challenge of integrating the system within pre-existing hull structures, without impacting hydrodynamic performance. And, in some cases, resolving challenges associated with limited volumetric space availability to house system components, e.g., air compressors. Further, existing auxiliary engine power is often limited, constraining the possibility of installing large-capacity air compressors.

2. Working Principle

2.1 Air Lubrication – A Short Literature Review

Hassan et al. (2006) reported that an increase in microbubble concentration leads to a reduction in the Reynolds stresses and turbulence production in the boundary layer (B.L.). *Sindagi et al. (2019)* stated that the drag reduced by microbubble drag reduction (MBDR) is due to alteration of the viscosity density of the fluid in the B.L. These changes reduce the Reynolds' stresses, which minimises shear stress. Work done by *Gao et al. (2023)* states that bubbles within the B.L. minimise the effect of formation and development of turbulence, if the air is injected into the laminar region.

The resultant net shear stress is reduced since the bubbles have lower shear stress than most solids. In some work, it is thought that the introduction of air reduces the overall viscosity of the B.L. and hinders turbulence production near the hull, *Stephani et al. (2006)*, *Hassan et al. (2008)*, and *Jiménez and Pinelli (1999)*.

Hassan and Gutiérrez-Torres (2006) reported that the increase of microbubbles within a B.L. is inversely proportional to the Reynolds stress. Reynolds stress measures the turbulent fluctuations in a fluid flow. It is responsible for the transfer of energy from large scales to small scales in fluid flow. This also holds for turbulence production. As more air is introduced, turbulence production is delayed,

Stephani et al. (2006).

According to *McCormick and Siddiqui (1989),* when bubbles split, they do so by extracting turbulence energy, therefore reducing turbulence. Turbulence energy is the amount of kinetic energy present in turbulent flow. It is measured in turbulent kinetic energy (TKE), and it is the sum of the kinetic energy associated with the velocity fluctuations, related to the Reynolds stress. TKE is generated by the action of large-scale velocity fluctuations, which are transferred to smaller scales via cascading. Later this was proven to be true when a particle image velocimetry (PIV) technique was used by *Jacob et al. (2010)*. Additionally, it was found that the flow velocity gradient changes in the turbulent layer. This could be because bubbles migrate into vortical structures thus disrupting them, *Sanders et al. (2006)*, *Murai (2014),* and *Elbing et al. (2008)*.

When the bubbles split, the diameter is reduced making the bubbles smaller. When the bubbles become smaller, they will be pushed away from the wall due to buoyancy effects and turbulent eddies. This will result in a restoration of the turbulent boundary layer (T.B.L.) and reduction of void fraction. As the smaller bubbles escape the T.B.L. further away from the injection point, only the larger bubbles will be left, leading to an overall reduction of void fraction and bubble concentration, *Kawamura et al. (2003)*. The higher the Reynolds number (Re), the higher the turbulence shearing effect and bubble breaking; therefore, bubble escaping will increase. This can result in a problem of persistence down stream of injection, *Pavlov et al. (2020)*.

Sanada et al. (2009) observed that the bubble trajectory and its place within the T.B.L. is strongly dependent on the Re. *Legendre et al. (2003)* used Direct Numerical Simulations (DNS) to model two spheres to study their relative motion and direction. It was concluded that direction and motion changed in accordance with the Re.

Kawamura et al. (2002) concludes that as the bubbles flow away from the injector they converge to an equilibrium value that is dependent on the local shear rate. Splitting takes places at around 1 – 10x the B.L. thickness while coalescence takes place at 100 x the B.L. thickness.

Work done by *Sindagi et al. (2019)* shows how the coefficient of friction (CF) increases further away from the injection both longitudinally and transversely as can be seen in Figure 1.

Kodama et al. (2002) showed that drag reduction in the spanwise direction is not uniform and it decreases further away from the centreline of injection. *Sanders et al. (2006)* and *Elbing et al. (2008)* reported that the drag reduction effect is lost the further downstream the drag is measured. This was thought to be due to the near-wall shears in the B.L.

This wall shear makes the bubbles move from the wall's surface. *Harleman (2012)* later confirmed this. Therefore, the shape with respect to the injection point is also an important parameter. *Jang et al. (2014)* did a study whereas a side wall of 10 mm height was put on a flat plate to avoid bubble escaping and using a side wall proved to be more effective.

As can be seen appreciated from this review any air injection into the boundary layer of a vessel will result in rather complex flow phenomena, not all of which can be completely resolved presently in any fluiddynamic simulations that accounts for the full-scale situation.

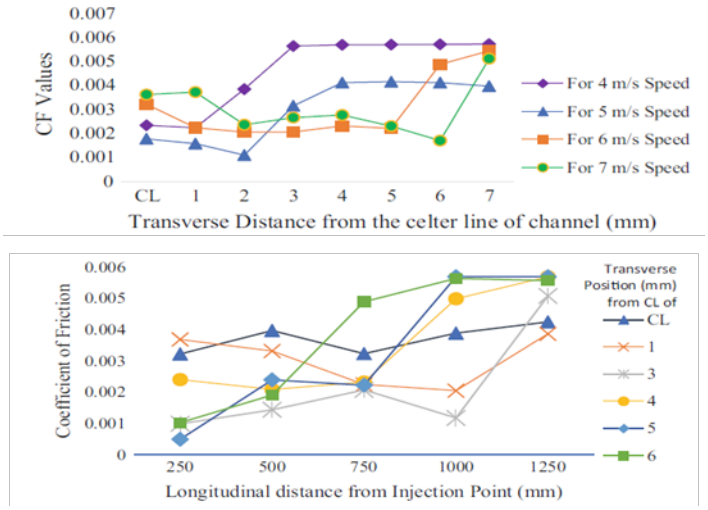

Figure 1: Increase of coefficient of friction with distance according to *Sindagi et al. (2019)*

2.2 Passive Air Lubrication System

Armada's Passive Air Lubrication System works on the Bernoulli principle and can be considered a naturally aspirated alternative to the active ALS currently on the market. The working principle uses the ship's forward motion to create a precise pressure differential between geometrically refined inlet and outlet transition pieces. This pressure differential develops the net driving force to 'power' the system.

As the ship moves forward, seawater enters the ship through a series of inlet transition pieces (the number varies depending on the application). The water transits through a low-pressure region (inline venturi subsystem), creating a net suction of air from deck level. Subsequently, a precise mixture of air and water is delivered downstream via an outlet transition piece back to the vessel boundary layer for optimal drag reduction performance.

Between each of the inlet and outlet transition pieces, the ejector (venturi) and a diffuser sit. The unique design of these sub-components allows for the development of a refined air-water ratio and a superior level of control of bubble size and homogeneity.

The PALS performance control system and machine learning capability support the system, which is designed with logic to tune the system set points to the prevailing vessel operating condition. An isometric view of the PALS is shown in Figure 2.

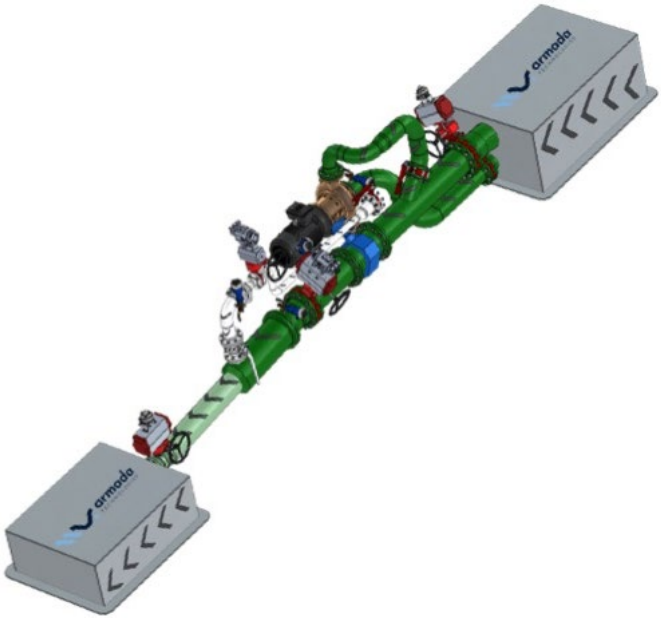

Figure 2: Isometric view of Armada's PALS

3. CFD Simulations

3.1 Global Simulations

3.1.1 CFD Methodology

The CFD simulations used for the geometry optimisation in this project have been run using a specialized and upgraded version of OpenFOAM®; details are given in *Renzsch et al. (2017)* and *Meyer et al. (2016)*. In this CFD code, the Reynolds-averaged Navier-Stokes equations (RANS) are solved on an unstructured grid using the finite volume method. Pressure velocity coupling uses the PIMPLE method, a combination of the SIMPLE, *Patankar and Spalding, (1972)*, and PISO methods, *Issa (1985)*.

Turbulent viscosity is computed using the k-ω-SST turbulence model, *Menter et al. (2003)*. The free surface is captured by applying the Volume-of-Fluid (VoF) method, *Hirt and Nichols (1981)*. The BRICS scheme, *Wackers et al. (2011)*, is used for convective transport of the VoF-scalar, providing compressive behaviour to keep the interface sharp. Bubble dynamics are disregarded; only the presence and amount of air underneath the hull are computed by this approach.

3.1.2 Case Setup Intake / Injector

To evaluate intake/injector properties and align with the tests conducted at HSVA (see section 4), the intake and injector are analysed and mounted in a channel with similar dimensions to HSVA's *Hydrodynamic and cavitation tunnel* (HyKaT). Figure 3 shows the injector and the balance plate arranged in the domain. The significant length upstream is intentional in allowing the boundary layer to fully develop.

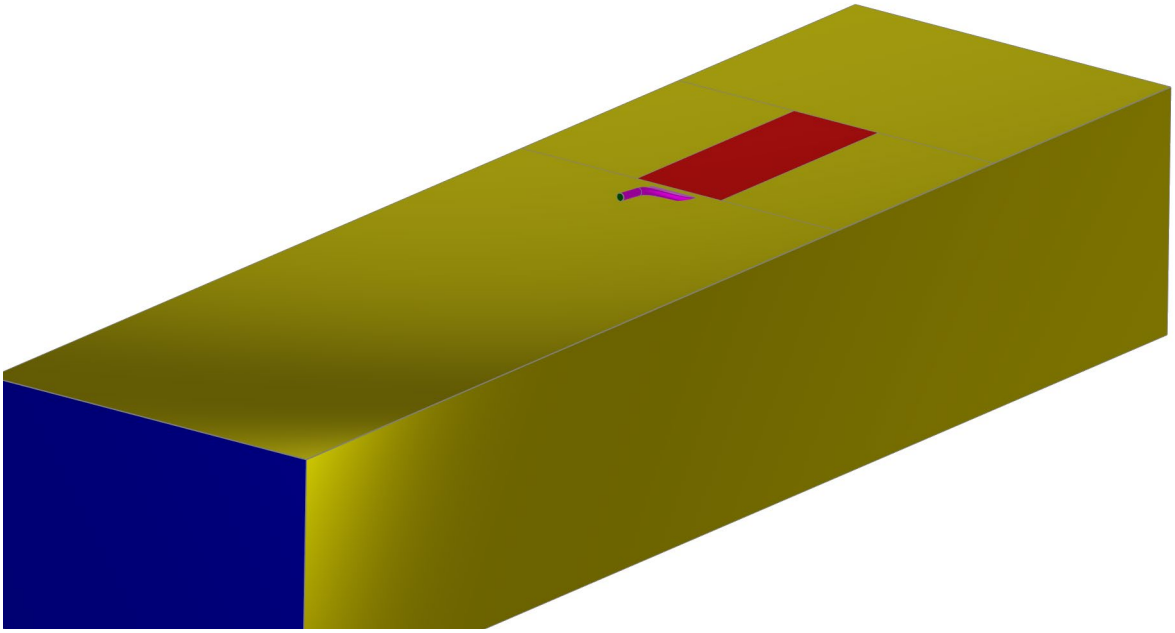

Figure 3: Schematic of injector and reference plate in domain

While the intake and injector geometries are parametrised (see section 5), design requirements fix basic dimensions like the system's length.

Due to the venturi pump's working principle and requirements, the volumetric flow rate (respectively velocity) at the inboard boundaries of intake and injector is prescribed. The pressure differential between the boundaries of intake and injector is monitored. One of the constraints during the optimisation is that a sufficient pressure differential must be maintained to drive the venturi pump.

To evaluate the quality of the air injection, the volume fraction on a plate downstream from the injector is monitored. Further, as a qualitative criterion, the stability of the air carpet is visually inspected, and geometries generating a highly transient behaviour are discarded from the optimisation process.

3.2 Simulations at Bubble Level

Experimental laboratory work done by *Qin et al. (2017)* shows oscillation in drag reduction due to bubble motion and behaviour, as seen in Figure 4. The graph depicts the coefficient of friction on the y-axis and the distance along the plate on the x-axis. As the air moves further down the plate, see section IV in Figure 4, the air turns into bubbles. This results in oscillating drag and lift due to the motions of the bubbles in the turbulent boundary layer (T.B.L.).

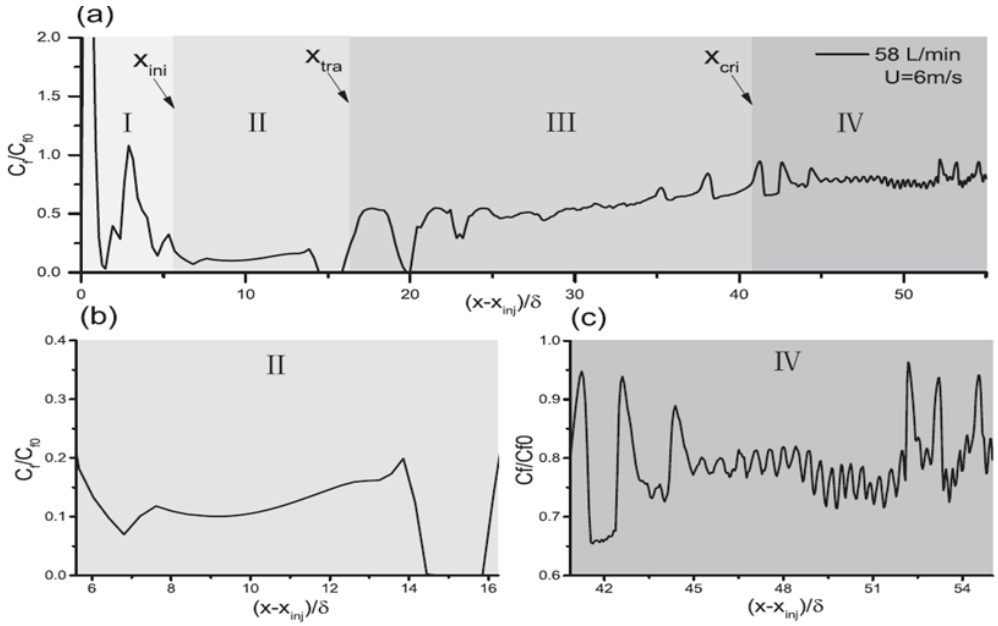

Figure 4: Bubble Oscillations Effect on drag reduction (D.R.), *Qin et al. (2017)*, with close-ups given in (b) and (c) for section II and section IV, respectively

The CFD simulations undertaken here also shows oscillating behaviour, as seen in Figure 5. Whilst numerical oscillations do occur, they do not happen at the same frequency and range. Hence, the behaviour of these oscillations is due to the air bubbles moving around in the T.B.L., giving confidence in the CFD model as it apparently captured such a tricky behaviour seen in experimental laboratory testing.

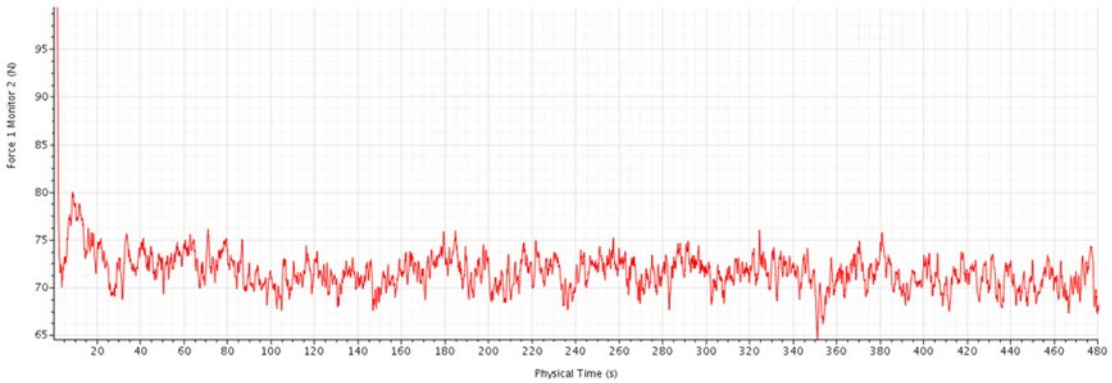

Figure 5: D.R. Across Modelled Plate with Oscillations

When the bubbles split, their diameter is reduced, making them smaller. As they become smaller, they will be pushed away from the wall due to buoyancy effects and turbulent eddies. This will result in a restoration of the T.B.L. and a reduction of the void fraction.

As the smaller bubbles escape the T.B.L. further away from the injection point, only the larger bubbles will be left, leading to an overall reduction of void fraction and bubble concentration, *Kawamura et al. (2003)*. The higher the Reynolds number, the higher the turbulence shearing effect and bubble breaking; therefore, bubble escaping will increase. This can result in a problem of persistence downstream of

injection *Pavlov et al. (2020)*.

Sanders et al. (2006) prove that the shear flow of the B.L. will not let the bubbles be in contact with the hull. The bubbles will be suspended at a location underneath the surface unless the bubbles coalesce and stratify. This thin layer of liquid between the hull and bubbles is sometimes called the "liquid layer" and can be seen in Figure 6, *Elbing et al. (2008)*.

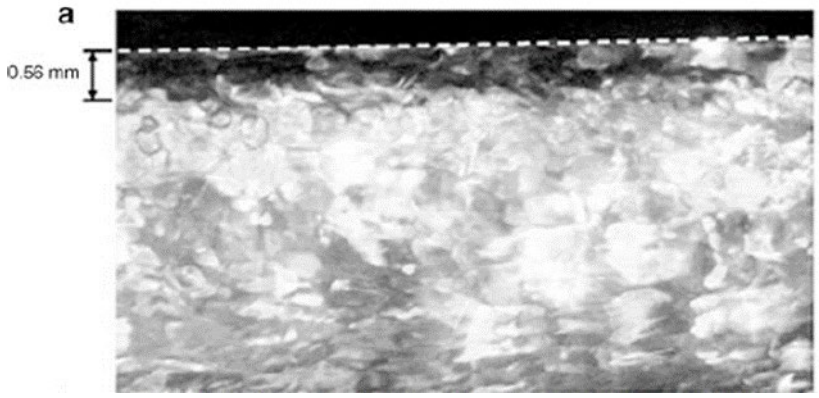

Figure 6: Observing the Liquid Layer, *Elbing et al. (2008)*

This is further explained in Figure 7. Part (a) shows how the B.L. is initially divided into a viscous sub-layer, buffer layer, outer layer, and flow region. Part (b) demonstrates how another layer is added, the bubbly two-phase layer between the outer and buffer layers, *Adrian (2007)*. This agrees with the findings from *Madavan et al. (1984)*, *Merkle et al. (1990)*, *Kanai and Miyata, (2001)*, and *Hassan et al. (2008),* where it was deduced that the concentration increases away from the wall up to a peak value and then decreases to zero once in the free stream.

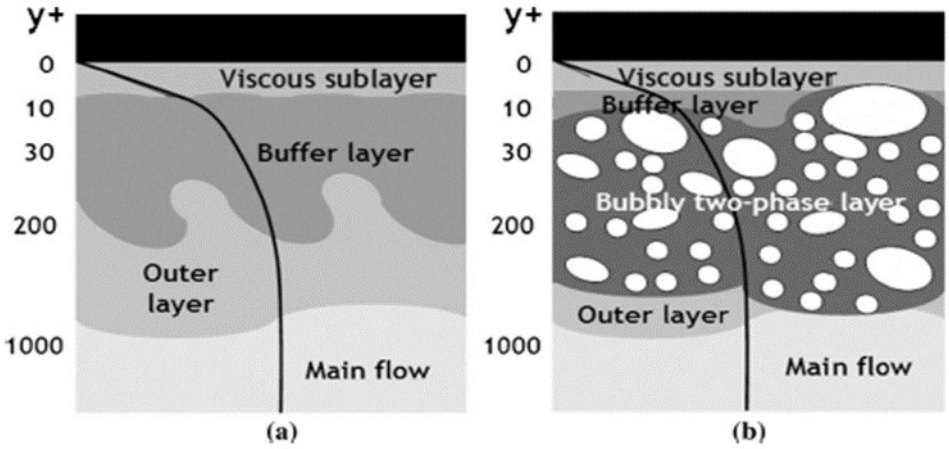

Figure 7: Boundary Layer with and Without Air Injection, *Adrian (2007)*

This also occurs in the CFD simulations, see Figure 8: The bubbles do not touch the flat plate, as mentioned in the literature previously and as can be seen in Figure 4 and Figure 5. This was noted across all models in same-plate testing, Reynolds-variance testing, and scaling-up testing. It further confirms the robustness of the CFD model and its ability to replicate sufficiently the air-water interaction behaviour observed in experiments.

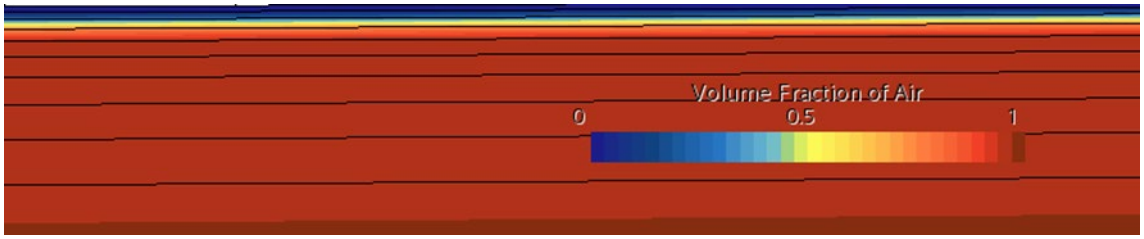

Figure 8: Liquid layer at the wall of the plate replicated by CFD

4. Experimental Testing

Armada Technologies has performed a series of targeted demonstration tests at the world-leading facility, HSVA, in Hamburg. HSVA not only operates the world's largest commercial cavitation tunnel (Hykat) but is also 'the' preeminent testing facility for Air Lubrication systems globally. Similarly, HSVA regularly attends sea trials of ALS to gain full-scale performance validation.

The test variables included:

1. Ship speed (represented by Hykat tunnel flow speed, in m/s)
2. Ship draught (represented by Hykat tunnel pressure, in kPa)
3. ATL water pump speed (m^3/hr)
4. ATL active air delivery rate (m^3/hr).

The results evidenced that the PALS design effectively introduced a layer of high-quality aerated water to the simulated vessel boundary layer. Similarly, complete passive aeration of PALS is achievable under the simulated operating conditions. The results indicate the existence of a drag reduction 'sweet spot' where two hydrodynamic phenomena are effectively balanced at every discreet operating condition, namely:

- The momentum balance between external and injected flow for favourable boundary layer behaviour.
- The optimal air-water-mixture ratio for best reduction of viscous resistance.

It was also identified that water injection alone already yields a certain drag reduction. Figure 9 gives an impression of the air bubbles coming out of the injector during the HyKaT experiments.

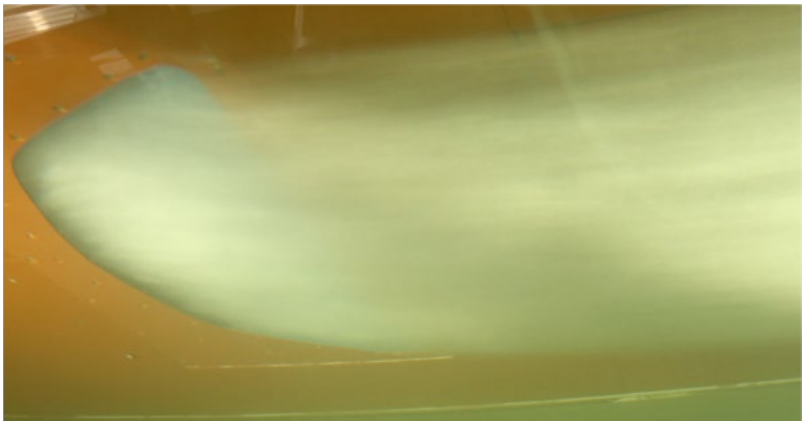
Figure 9: Air bubbles being injected during HyKaT experiments

5. Parametric Models and Geometry Optimisation

When optimizing a product, the effort of exploring the design space and exploiting the potential for further improvement scales up rapidly with the number of free variables of the systems, i.e., the degree of freedom (DoF). The more free variables, the more variants are needed, *Harries (2020)*.

Consequently, a deliberate variability reduction is built into a system instead of allowing any

conceivable freedom. This is usually realised by defining a product with as few descriptors, typically called parameters, as possible. In Computer-Aided Design (CAD), this approach is generally referred to as parametric modelling. In this study, the Process Integration and Design Optimisation platform CAESES® by Friendship Systems has been used for parametric modelling, design space exploration, and optimisation.

5.1 Intake / Injector

As first step the intake (whose task it is to provide sufficient dynamic pressure at for the venturi at a given flow rate) and the injector which in turn shall create an efficient bubble distribution downstream are optimised.

A fully-parametric approach has been chosen for both the intake and the injector to provide large design flexibility within the intended design space. This approach allows for the variation of all relevant angles, distances, radii, and cross-sections with a very low number of design variables. Figure 10 shows a generic representation of the injector model. It is worth noting that the fully-parametric model is the same for both intake and injector but the target functions differ.

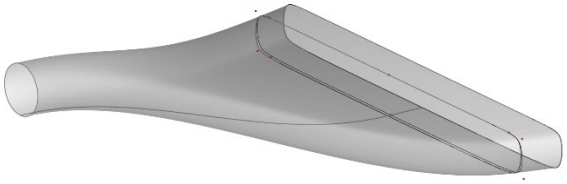

Figure 10: Generic representation of parametric injector model

First, the plausible design space is evaluated to optimise intake and injector geometry. This is achieved using a Sobol distribution of the variables within the parameter bounds. Approximately 60 variants are required to characterise the design space properly for six free variables. Based on this description, a response surface model is set up to search for actual optima. Here, another six variants were required until reaching the point of diminishing returns.

Having optimised the geometry of the intake and the injector, respectively, for generic set-ups situations that are representative of the flow situation encountered beneath the hull, an individual arrangement has to be found for each specific hull form to benefit from the PALS the most.

5.2 Arrangement

First, the hull geometry was imported into CAESES and kept fixed to model and optimise the arrangement of the PAL systems. Five optimised systems (optimised as discussed above) were placed in the vessel, with locations described by parameters giving longitudinal and transversal positions. Constraints were placed on the possible locations to take the vessel's geometric limitations into account and avoid interference between the systems. A generic arrangement is shown in Figure 11.

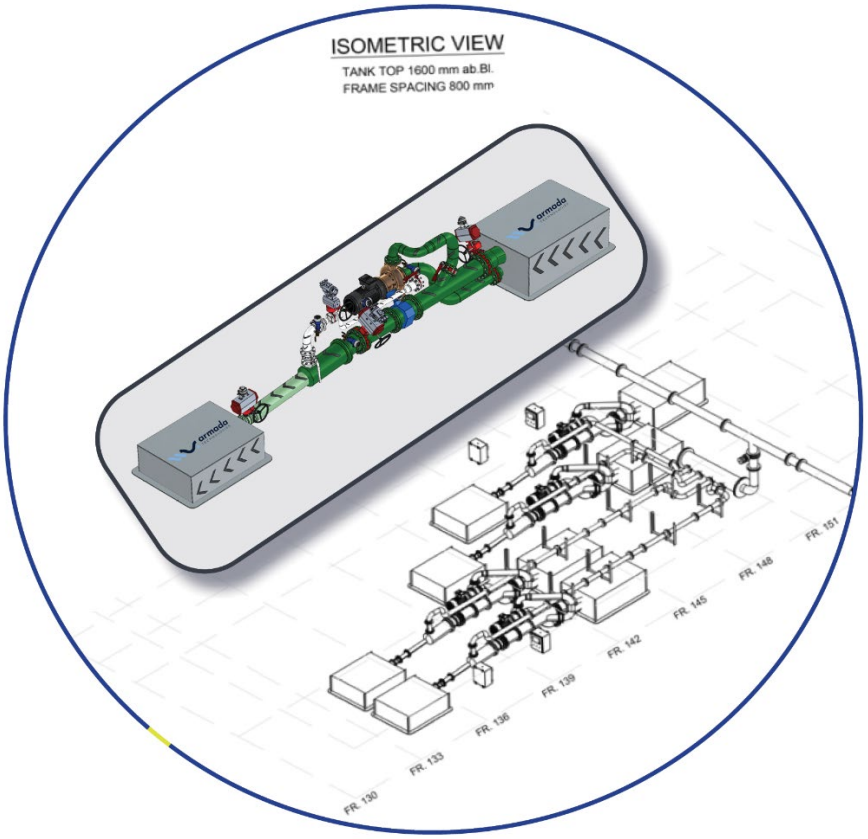

Figure 11: Generic arrangement in vessel

While the vessel's structure dictated discrete steps in the possible locations of some places, this does not lend itself well to numerical optimisation approaches. Therefore, the arrangement was initially optimised in a continuous design space (within the constraints), and moved to the nearest feasible location afterwards.

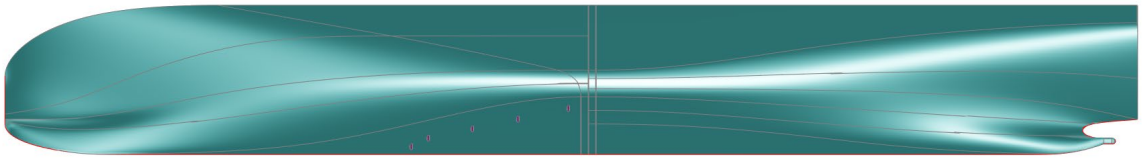

Figure 12: Global view on initial arrangement in vessel

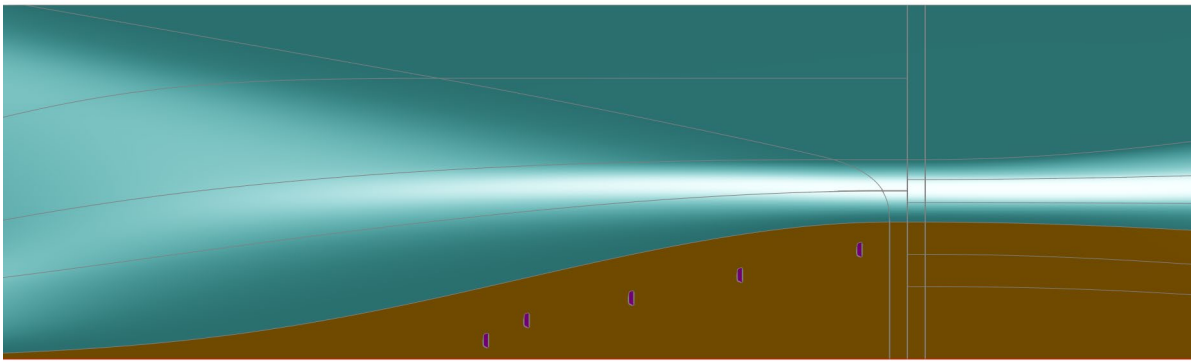

Figure 13: Close-up of initial arrangement and permissible installation region (gold)

Figure 12 gives a global overview of the vessel investigated in this study and the initial arrangement before optimisation. In the close-up shown in Figure 13, the permissible region – the flat of bottom – is depicted in gold.

The optimisation approach is similar to that used previously for the intake/injector. A total of 70 variants were used to explore the design space and 15 for the response surface-based optimisation.

6. Exemplary Results

6.1 Intake / Injector

The design space exploration and subsequent optimisation of the injector's shape have shown that the bubble distribution downstream highly depends on the injector's shape. In Figure 14 some unfavourable bubble distributions are shown: While some geometries introduce narrow but highly concentrated bubble streams (a), others may create oscillations due to destabilising the boundary layer (b), or a highly inhomogeneous distribution (c). Ideally, a wide-spread, stable bubble stream with sufficiently high and homogeneous concentration is sought (Figure 15). With the same amount of air injected, the improvement in air coverage of the balance plate from worst to best is 15%.

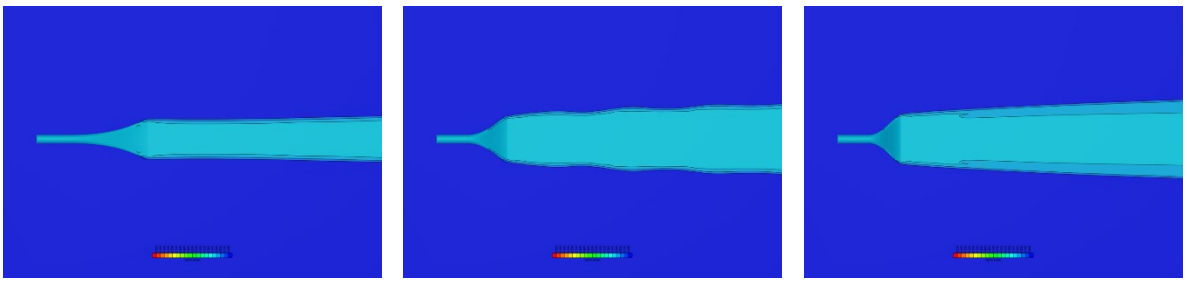

(a) narrow (b) unstable (c) inhomogeneous

Figure 14: Unfavourable bubble distributions

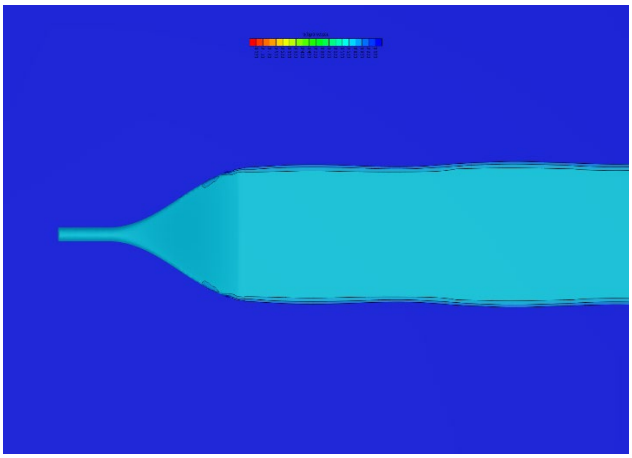

Figure 15: Favourable bubble distribution

6.2 Arrangement

Besides the obvious question on overall longitudinal installation – is it favourable to have the systems as far forward as possible to maximise covered length or is there too much air lost by disturbances due to crossflow across the forward bilge? – the quality of the air bubble coverage appears to be a determining factor.

On this particular hull shape (low block coefficient c_B), a far-aft installation (Figure 16) can harm

coverage quality as the bubbles enter the lower-speed thick boundary layer region aft before the sheet stabilises.

In the optimised installation (Figure 17), only the innermost systems are brought forward and inboard significantly. Even though a gap appears in the bubble carpet, the bubble coverage on the stern gondola is improved.

Figure 16: Far-aft installation arrangement

Figure 17: Optimised arrangement

7. Conclusions

The challenge of reducing emissions in merchant shipping is pressing, driven by recent and impending regulations. For existing vessels, options are limited, making solutions such as air lubrication systems (ALS) vital. Integrating ALS into existing ships poses significant challenges, including space constraints and potentially additional engine power.

Armada's Passive Air Lubrication System (PALS) operates using the Bernoulli principle, relying on the ship's motion to generate the necessary pressure differential for system operation. This innovative approach mitigates the need for large-capacity air compressors, making it suitable for retrofitting existing vessels. Instead, by utilising the dynamic pressure head from the vessels forward motion the power to drive the venturi pump is provided by the main engine. While this results in a small increase of pressure drag the air bubbles yield a significantly larger reduction of viscous drag, giving a net reduction of total resistance. Computational Fluid Dynamics (CFD) simulations, utilising advanced models and methodologies, play a crucial role in optimising the system's components and evaluating performance.

Experimental tests at HSVA validated PALS, demonstrating effective drag reduction by creating a high-quality aerated layer. The tests identified an optimal balance of hydrodynamic phenomena that maximises drag reduction at specific operating conditions. Additionally, parametric modelling and optimisation were employed to refine the intake and injector designs, ensuring efficient bubble distribution and system arrangement within the vessel.

Overall, the development and optimisation of PALS through a combination of CFD simulations and experimental testing offer a promising solution to reduce fuel consumption and, hence, emissions in existing merchant ships, addressing regulatory requirements and contributing to more sustainable maritime operations.

Acknowledgements

This research was funded by project "RETROFIT solutions to achieve 55% GHG reduction by 2030" (RETROFIT55) - Horizon Europe programme, Grant Agreement No. 1011096068".

References

ADRIAN, R.J. (2007), *Hairpin vortex organization in wall turbulence*, Physics of Fluids 19(4). doi:10.1063/1.2717527

ELBING, B.R., CECCIO, S.L., WINKEL, E.S., PFLUEGER, A.J., MEINHART, C.D., PERLIN, M., DOWLING, D.R. (2008), *Bubble-induced skin-friction drag reduction and the abrupt transition to air-layer drag reduction*, Journal of Fluid Mechanics 612(May), pp.201-236. doi:10.1017/S0022112008003029

GAO, Q., XU, J., WANG, Z., ZHANG, L., MA, Y., FENG, J. (2023), *Experimental study on bubble drag reduction by the turbulence suppression in bubble flow*, Ocean Engineering 272(February), p.113804. doi:10.1016/j.oceaneng.2023.113804

HARLEMAN, M.J. (2012), *On the effect of turbulence on bubbles: experiments and numerical simulations of bubbles in wall-bounded flows*, Ph.D. Thesis, TU Delft, The Netherlands

HARRIES, S. (2020), *Practical shape optimization using CFD: state-Of-The-Art in industry and selected trends*, Conference on computer applications and information technology in the maritime industries (COMPIT), Pontignano, Italy

HASSAN, Y.A., GUTIÉRREZ-TORRES, C.C. (2006), *Investigation of drag reduction mechanism by microbubble injection within a channel boundary layer using particle tracking velocimetry*, Nuclear Engineering and Technology 38(8), pp.763-778

HASSAN, Y.A., GUTIÉRREZ-TORRES, C.C., BARBOSA-SALDAÑA, J.G., JUÁREZ-BADILLO, J.A. (2008), *Drag reduction by microbubble injection in a channel flow*, Revista Mexicana de Física 54(1), pp.8-14

HIRT, C.W., NICHOLS, B.D. (1981), *Volume of fluid (VOF) method for the dynamics of free boundaries*, Journal of Computational Physics, 1/39

IMO (2023), *IMO strategy on reduction of GHG emissions from ships*, MEPC.377(80)

ISSA, R.I. (1985), *Solution of the Implicitly Discretized Fluid Flow Equations by Operator-Splitting*, Journal of Computational Physics, 62, pp.40-65

JACOB, B., ANDERSON, W.A., BELWARD, J.A. (2010), *Drag reduction by microbubbles in a turbulent boundary layer*, Physics of Fluids 22(115104). doi:10.1063/1.3492463

JANG, J., LEE, S.J., LEE, D.K., YOU, D.J., OH, S.J., LEE, I. (2014), *Experimental investigation of frictional resistance reduction with air layer on the hull bottom of a ship*, International Journal of Naval Architecture and Ocean Engineering 6(2), pp.363-379. doi:10.2478/IJNAOE-2013-0185

JIMÉNEZ, J., PINELLI, A. (1999), *The autonomous cycle of near-wall turbulence*, Journal of Fluid Mechanics 389, pp.335-359. doi:10.1017/S0022112099005066

KANAI, A., MIYATA, H. (2001), *Direct numerical simulation of wall turbulent flows with microbubbles*, International Journal for Numerical Methods in Fluids 35(5), pp.593-615

KAWAMURA, T., KAKUGAWA, A., KODAMA, Y. (2002), *Controlling the size of microbubbles for drag reduction*, 3rd Symposium on Smart Control of Turbulence. Available at: http://www.nmri.go.jp/turbulence/PDF/symposium/FY2001/Kawamura.pdf

KAWAMURA, T., TAKAHASHI, T., KODAMA, Y., KAKUGAWA, A., TAKEDA, H. (2003), *Effect*

of bubble size on the microbubble drag reduction of a turbulent boundary layer, Proceedings of the ASME/JSME Joint Fluids Engineering Conference 2A, pp.647-654. doi:10.1115/fedsm2003-45645

KODAMA, Y., KAKUGAWA, A., TAKAHASHI, T., NAGAYA, S., SUGIYAMA, K. (2002), *Microbubbles: drag reduction mechanism and applicability to ships*, in 24th Symp. Naval Hydrodynamics, pp.1-19

LEGENDRE, D., MAGNAUDET, J., MOUGIN, G. (2003), *Hydrodynamic interactions between two spherical bubbles rising side by side in a viscous liquid*, Journal of Fluid Mechanics 497, pp.133-166. doi:10.1017/S0022112003006463

MADAVAN, N.K., DEUTSCH, S., MERKLE, C.L. (1984), *Reduction of turbulent skin friction by microbubbles*, Physics of Fluids 27(2), pp.356-363. doi:10.1063/1.864620

McCORMICK, J.M., SIDDIQUI, M.U. (1989), *Microbubble formulation and splitting in a turbulent boundary layer for turbulence reduction*, in Advances in Fluids Dynamics, pp.168-217

MENTER, F.R., KUNTZ, M., LANGTRY, R. (2003), *Ten Years of Industrial Experience with the SST Turbulence Model*, Turbulence, Heat and Mass Transfer 4, ed: K. Hanjalic, Y. Nagano, M. Tummers, Begell House, Inc., pp.625-632

MERKLE, C.L., DEUTSCH, S. (1990), *Drag Reduction in liquid boundary layers by gas injection*, in The Smithsonian/NASA Astrophysics Data System, pp.351-412. doi:10.2514/4.865978

MEYER, J., RENZSCH, H., GRAF, K., SLAWIG, T. (2016), *Advanced CFD-Simulations of free-surface flows around modern sailing yachts using a newly developed OpenFOAM solver*, The 22nd Chesapeake Sailing Yacht Symposium, Annapolis, MD, USA

MURAI, Y. (2014), *Frictional drag reduction by bubble injection*, Experiments in Fluids 55(7). doi:10.1007/s00348-014-1773-x

PAVLOV, G.A., ORLOVA, I.P., KUDRYAVTSEV, I.V., PAVLOVA, M.V. (2020), *Air Lubricated and Air Cavity Ships*, Springer. doi:10.1007/978-1-0716-0425-0

QIN, S., OKA, Y., TAKAHASHI, H., FUKUDA, K. (2017), *Stream-wise distribution of skin-friction drag reduction on a flat plate with bubble injection*, Physics of Fluids 29(3). doi:10.1063/1.4977800

RENZSCH, H.; MEYER, J.; GRAF, K. (2017), *Investigation of Modern Sailing Yachts Using a New Free-Surface RANSE Code*, International Conference on Innovation in High Performance Sailing Yachts, Lorient, FR

SANADA, T., IGUCHI, M., NAKATANI, A., YOSHIDA, T. (2009), *Motion and coalescence of a pair of bubbles rising side by side*, Chemical Engineering Science 64(11), pp.2659-2671. doi:10.1016/j.ces.2009.02.042

SANDERS, W.C., WINKEL, E.S., DOWNING, D.R., PERLIN, M., CECCIO, S.L. (2006), *Bubble friction drag reduction in a high-Reynolds-number flat-plate turbulent boundary layer*, Journal of Fluid Mechanics 552, pp.353-380. doi:10.1017/S0022112006008688

SINDAGI, S., DASH, S.K., BANERJEE, J., RAMESH, O. (2019), *Numerical investigation of influence of microbubble injection, distribution, void fraction and flow speed on frictional drag reduction*, Lecture Notes in Civil Engineering, Springer Singapore. doi:10.1007/978-981-13-3119-0_17

STEPHANI, K.A., BEUTNER, T.L., WITTMER, K., BUSHNELL, D.M. (2006), *Drag Reduction*

using Trapped Bubbles on a Flat Plate Surface, in American Institute of Aeronautics and Astronautics, pp.1-19

WACKERS, J., KOREN, B., RAVEN, H.C., VAN DER PLOEG, A., STARKE, A.R., DENG, G.B., QUEUTEY, P., VISONNEAU, M., HINO, T., OHASHI, K. (2010), *Free-surface viscous flow solution methods for ship hydrodynamics*, Archives of Computational Methods in Engineering 18, pp.1-41